

Theoretical investigation of braking of tearing mode rotation by resistive walls in ITER F

Cite as: Phys. Plasmas **30**, 042514 (2023); <https://doi.org/10.1063/5.0141742>

Submitted: 08 January 2023 • Accepted: 21 March 2023 • Published Online: 17 April 2023

 R. Fitzpatrick

COLLECTIONS

F This paper was selected as Featured



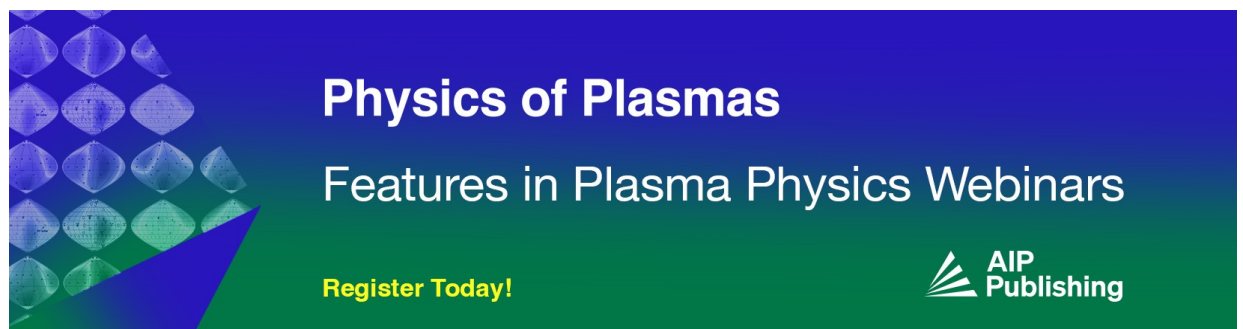
View Online



Export Citation




CrossMark



Physics of Plasmas
Features in Plasma Physics Webinars

Register Today!



Theoretical investigation of braking of tearing mode rotation by resistive walls in ITER

Cite as: Phys. Plasmas **30**, 042514 (2023); doi: [10.1063/5.0141742](https://doi.org/10.1063/5.0141742)

Submitted: 8 January 2023 · Accepted: 21 March 2023 ·

Published Online: 17 April 2023



View Online



Export Citation



CrossMark

R. Fitzpatrick^{a)} 

AFFILIATIONS

Institute for Fusion Studies, Department of Physics, University of Texas at Austin, Austin, Texas 78712, USA

^{a)} Author to whom correspondence should be addressed: rfitzp@utexas.edu

ABSTRACT

The locking of the 2/1 tearing mode to the resistive wall in the ITER tokamak (15 MA inductive scenario 2) is investigated theoretically using a cylindrical asymptotic matching model. The model takes into account the fact that ITER plasmas will effectively be surrounded by two walls; the inner blanket module layer with a time constant of about 23 ms, and the outer vacuum vessel with a time constant of about 380 ms. The model also takes cognizance of the fact that neither the blanket module layer nor the vacuum vessel can be accurately described as “thin” walls (in the ordinarily accepted sense). The model incorporates changes in both the plasma poloidal and the toroidal angular velocity profiles, in response to the electromagnetic braking torque that develops at the rational surface, because it turns out that neoclassical poloidal flow-damping is not strong enough to completely suppress changes in the poloidal velocity. Finally, the model accurately calculates changes in the poloidal and toroidal plasma angular velocity profiles by evolving the full angular equations of motion, taking the electromagnetic braking torque, plasma inertia, plasma viscosity, and poloidal flow-damping into account. The time required for the 2/1 tearing mode to grow from a small amplitude to a sufficient one to lock to the walls is found to be about 3.5 s. The critical full radial island width at which wall locking is triggered is found to be about 9% of the plasma minor radius.

Published under an exclusive license by AIP Publishing. <https://doi.org/10.1063/5.0141742>

I. INTRODUCTION

A rotating tearing mode in a tokamak plasma induces helical eddy currents in surrounding, rigid, electrically conducting structures, such as the vacuum vessel, that lead to the development of an electromagnetic braking torque acting on the plasma that slows down the mode's rotation. In fact, if the mode grows to sufficiently large amplitude, then its rotation is effectively arrested, i.e., it “locks” to the surrounding structures.^{1–7} This phenomenon is a cause for concern because there is a strong empirical correlation between locked tearing modes and disruptions in tokamak discharges.⁸

Given that disruption avoidance is crucial to the success of the ITER project, it is clearly important to develop an accurate model for predicting the critical tearing mode amplitude (which is most conveniently parameterized in terms of the full radial width of the associated magnetic island chain that develops at the rational surface inside the plasma⁶) at which mode locking will take place in ITER discharges. It is also important to accurately model the time interval between the onset of the mode and the occurrence of mode locking, as this must be taken into account when designing control strategies to suppress tearing modes.⁹

ITER plasmas will be surrounded by a relatively distant (i.e., $r_v/a \simeq 1.5$, where r_v and a are the minor radii of the vessel and the

plasma, respectively), double, vacuum vessel fabricated from austenitic stainless steel, type 316L(N)-IG, with an electrical resistivity of $\eta_v = 7.4 \times 10^{-7} \Omega \text{ m}$.¹⁰ A 3D model (with port openings) of the vacuum vessel has revealed that the longest decay time of $n = 1$ (where n is a toroidal mode number) eddy currents flowing in the double structure, in the absence of plasma, is $\tau_d = 188 \text{ ms}$.^{11,12} According to cylindrical theory,⁶ this decay time is related to the so-called time-constant of the vessel, which (in this paper) is defined as $\tau_v = \mu_0 r_v \delta_v / \eta_v$, where δ_v is the effective radial thickness of the vessel, according to $\tau_d = \tau_v / (2m)$, where m is a poloidal mode number. (Note that another common convention used in the literature defines the time constant to be $\mu_0 r_v \delta_v / 2\eta_v$, i.e., half of that in this paper.) Hence, assuming that the most slowly decaying eddy current is characterized by $m = 1$, we deduce that $\tau_v = 376 \text{ ms}$.

The region between the edge of an ITER plasma and the vacuum vessel will be occupied by a layer of blanket modules.¹⁰ These modules will be fabricated from boronated stainless steel blocks with complicated 3D structures, which are designed to shield the surrounding regions from neutrons generated within the plasma. A thin first-wall fabricated from a beryllium layer, followed by a copper layer, and a stainless steel layer will be attached to the inner surfaces of the blocks.

Detailed 3D modeling of the blanket module layer (including the first-wall) has revealed that, as far as its interaction with non-rotating resistive wall modes is concerned, it acts like a simple resistive wall in which the ratio of the electrical resistivity, η_b , to the wall thickness, δ_b , takes the value $\eta_b/\delta_b = 1.33 \times 10^{-4} \Omega$ (see Sec. 4.4 and Fig. 9 in Ref. 13). Given that the inner radius of the blanket modules will lie at $r_b/a \simeq 1.2$, and that $a = 2.0$ m for ITER, we deduce that the effective time-constant of the blanket module layer is $\tau_b = \mu_0 \times 1.2 \times 2.0 / 1.33 \times 10^{-4} = 23$ ms. Note that this time-constant is much less than that of the vacuum vessel.

A recent calculation of the slowing down and locking of tearing modes in ITER, performed by La Haye, Paz-Solden, and Liu, that takes the blanket modules into account, has shown that the $m = 2/n = 1$ tearing mode, which is generally considered to be the most dangerous mode, can slow down and lock-in about 3 s.¹⁴ Moreover, the critical island width at which locking occurs is predicted to be about 9 cm, which corresponds to 4.5% of the plasma minor radius. The latter prediction is alarming because tearing modes in existing (large) tokamak plasmas only lock when their widths exceed about 10% of the plasma minor radius.¹⁴ In other words, the new calculation implies that ITER plasmas are likely to be far more susceptible to disruption-triggering locked modes than plasmas in existing (large) tokamaks.

The calculation of La Haye *et al.* is ultimately based on the cylindrical analysis of Nave and Wesson.⁴ The calculation only takes the blanket module layer into account. Moreover, the blanket module layer is treated as a thin wall, which means that the skin-depth in the wall material is assumed to be much greater than the wall thickness. The calculation neglects any changes in the plasma poloidal angular velocity profile, in response to the electromagnetic braking torque that develops at the rational surface, on the assumption that such changes are completely suppressed by neoclassical poloidal flow-damping.⁴ The calculation only models the evolution of the plasma toroidal angular velocity profile, under the influence of the electromagnetic braking torque, plasma inertia, and plasma viscosity, in a highly approximate manner. Finally, the values of some important parameters in the model (i.e., C_w and C_M) are determined by empirical fitting to experimental DIII-D data rather than from theory.

The aim of this paper is to perform a purely theoretical (i.e., with no empirical fitting) version of the calculation of La Haye *et al.*, which takes more physics into account. Given the alarming implications of the La Haye calculation for ITER, this seems like a worthwhile exercise. Our calculation is ultimately based on the cylindrical asymptotic matching model of Fitzpatrick,⁶ but will take into account the presence of both the blanket module layer and the vacuum vessel. We shall also take cognizance of the fact that neither the blanket module layer nor the vacuum vessel can be accurately described as thin walls.¹⁵ Our calculation incorporates changes in both the plasma poloidal and the toroidal angular velocity profiles, in response to the electromagnetic braking torque that develops at the rational surface, because it turns out that neoclassical poloidal flow-damping is not strong enough to completely suppress changes in the poloidal velocity (see Fig. 3). Finally, we shall accurately model the changes in the poloidal and toroidal plasma angular velocity profiles by evolving the full angular equations of motion, taking the electromagnetic braking torque, plasma inertia, plasma viscosity, and poloidal flow-damping into account. Note that a similar, but somewhat simpler, version of the theoretical model employed in this paper was able to successfully model

the slowing down and locking of large amplitude $m = 1$ tearing modes to a thick wall in the MST reversed field pinch.⁷

II. DERIVATION OF ROTATION BRAKING EQUATIONS

A. Plasma equilibrium

Consider a low- β , large aspect-ratio, tokamak plasma equilibrium whose magnetic flux-surfaces map out (almost) concentric circles in the poloidal plane. Such an equilibrium can be approximated as a periodic cylinder.⁶ Let us employ a conventional set of right-handed cylindrical coordinates, r , θ , and z . The equilibrium magnetic flux-surfaces lie on surfaces of constant r . The system is assumed to be periodic in the z (“toroidal”) direction, with periodicity length $2\pi R_0$, where R_0 is the simulated major radius of the plasma. Let a be the minor radius of the plasma. The equilibrium magnetic field is written $\mathbf{B} = B_\theta(r) \mathbf{e}_\theta + B_\varphi \mathbf{e}_z$, where $B_\theta(r)$ is the poloidal magnetic field-strength and B_φ is the (approximately) spatially uniform toroidal magnetic field-strength. The safety-factor profile takes the form $q(r) = r B_\varphi / [R_0 B_\theta(r)]$. The equilibrium current density is written $\mathbf{j} = j_\varphi(r) \mathbf{e}_z$, where $\mu_0 j_\varphi(r) = (B_\varphi/R_0) J_\varphi(r)$. Here, the dimensionless function $J_\varphi(r) = (1/r) (r^2/q)'$, with $' \equiv d/dr$, parameterizes the toroidal plasma current density profile.

B. Tearing mode perturbation

Consider helical tearing mode instability with m periods in the poloidal direction and n periods in the toroidal direction.¹⁶ The perturbed magnetic field associated with the tearing mode can be written as⁶

$$\frac{\delta B_r}{R_0 B_\varphi} \simeq i \frac{m}{r} \psi, \quad (1)$$

$$\frac{\delta B_\theta}{R_0 B_\varphi} \simeq -\psi', \quad (2)$$

$$\frac{\delta B_\varphi}{R_0 B_\varphi} \simeq \frac{n}{R_0} \frac{r}{m} \psi' - \frac{n}{R_0} \frac{r}{m} \frac{J_\varphi \psi}{r(1/q - n/m)}. \quad (3)$$

Here, the dimensionless function $\psi(r, t)$ parameterizes the perturbed helical magnetic flux. Furthermore, there is an implicit $\exp[i(m\theta - n\varphi)]$ variation of perturbed quantities, where $\varphi = z/R_0$ is the toroidal angle. Finally, we have made use of the standard large aspect-ratio tokamak orderings that $r/R_0 \ll 1$ and $q \sim \mathcal{O}(1)$. The perturbed plasma current density associated with the tearing mode can be written as⁶

$$\frac{\mu_0 \delta j_r}{R_0 B_\varphi} \simeq -i \frac{n}{R_0} \frac{J_\varphi \psi}{r(1/q - n/m)}, \quad (4)$$

$$\frac{\mu_0 \delta j_\theta}{R_0 B_\varphi} \simeq \frac{n}{R_0} \frac{m}{r} \psi - \frac{n}{R_0} \frac{r}{m} \frac{(r\psi)'}{r} + \frac{n}{R_0} \frac{r}{m} \frac{1}{r} \left[\frac{J_\varphi \psi}{1/q - n/m} \right]', \quad (5)$$

$$\frac{\mu_0 \delta j_\varphi}{R_0 B_\varphi} \simeq \frac{m^2}{r^2} \psi - \frac{(r\psi)'}{r}. \quad (6)$$

The tearing mode perturbation satisfies the perturbed force balance equation $\delta \mathbf{j} \times \mathbf{B} + \delta \mathbf{B} \times \mathbf{j} \simeq \nabla \delta p$, where δp is the perturbed plasma pressure.¹⁶ The z -component of the curl of this equation yields the well-known cylindrical tearing mode equation,^{6,17}

$$\frac{\partial^2 \psi}{\partial r^2} + \frac{1}{r} \frac{\partial \psi}{\partial r} - \frac{m^2}{r^2} \psi - \frac{J'_\varphi \psi}{r(1/q - n/m)} = 0. \quad (7)$$

Note that this equation is singular at the so-called rational magnetic flux-surface, radius r_s , at which $q(r_s) = m/n$.

In general, the physical solution of Eq. (7) that is well behaved at $r=0$ and satisfies appropriate boundary conditions at $r=a$ is such that ψ is continuous across the rational surface, whereas $\partial\psi/\partial r$ is discontinuous.¹⁶ The complex dimensionless quantity

$$\Psi_s(t) = \psi(r_s, t), \quad (8)$$

parameterizes the amplitude and phase of the reconnected magnetic flux at the rational surface, whereas the complex dimensionless quantity

$$\Delta\Psi_s(t) = \left[r \frac{\partial \psi}{\partial r} \right]_{r_s^-}^{r_s^+}, \quad (9)$$

parameterizes the amplitude and phase of a helical current sheet that flows (parallel to the equilibrium magnetic field) at the rational surface.

C. Resistive walls

Suppose that the plasma is surrounded by two concentric, thin (compared to their minor radii, but not necessarily compared to their skin-depths) resistive walls of radii r_b and r_v , where $a < r_b < r_v$. The inner wall represents the blanket modules, whereas the outer wall represents the vacuum vessel. The tearing perturbation in the vacuum region outside the plasma (i.e., the region $r > a$), excluding the walls, satisfies Eq. (7) with $J_\varphi = 0$. The complex dimensionless quantity

$$\Psi_b(t) = \psi(r_b, t), \quad (10)$$

parameterizes the amplitude and phase of the perturbed magnetic flux that penetrates the inner wall, whereas the complex dimensionless quantity

$$\Delta\Psi_b(t) = \left[r \frac{\partial \psi}{\partial r} \right]_{r_b^-}^{r_b^+}, \quad (11)$$

parameterizes the amplitude and phase of a helical eddy current sheet that flows (parallel to the equilibrium magnetic field at the rational surface) in the inner wall. Likewise, the complex dimensionless quantity

$$\Psi_v(t) = \psi(r_v, t), \quad (12)$$

parameterizes the amplitude and phase of the perturbed magnetic flux that penetrates the outer wall, whereas the complex dimensionless quantity

$$\Delta\Psi_v(t) = \left[r \frac{\partial \psi}{\partial r} \right]_{r_v^-}^{r_v^+}, \quad (13)$$

parameterizes the amplitude and phase of a helical eddy current sheet that flows (parallel to the equilibrium magnetic field at the rational surface) in the outer wall.

D. Asymptotic matching

The most general physical solution of the cylindrical tearing mode equation, Eq. (7), can be written as¹⁸

$$\psi(r, t) = \Psi_s(t) \psi_s(r) + \Psi_b(t) \psi_b(r) + \Psi_v(t) \psi_v(r), \quad (14)$$

where $\psi_s(0) = 0$, $\psi_s(r_s) = 1$, $\psi_s(r \geq r_b) = 0$, $\psi_b(r \leq r_s) = 0$, $\psi_b(r_b) = 1$, $\psi_b(r \geq r_v) = 0$, $\psi_v(r \leq r_b) = 0$, $\psi_v(r_v) = 1$, and $\psi_v(\infty) = 0$. Here, $\psi_s(r)$, $\psi_b(r)$, and $\psi_v(r)$ are the real continuous functions that have gradient discontinuities at $r = r_s$, $r = r_b$, and $r = r_v$. It is helpful to define the real dimensionless quantities¹⁸

$$E_{ss} = \left[r \frac{d\psi_s}{dr} \right]_{r_s^-}^{r_s^+}, \quad (15)$$

$$E_{bs} = - \left[r \frac{d\psi_s}{dr} \right]_{r_b^-}, \quad (16)$$

$$E_{sb} = \left[r \frac{d\psi_b}{dr} \right]_{r_s^+}, \quad (17)$$

$$E_{bb} = \left[r \frac{d\psi_b}{dr} \right]_{r_b^-}^{r_b^+}, \quad (18)$$

$$E_{vb} = - \left[r \frac{d\psi_b}{dr} \right]_{r_v^-}, \quad (19)$$

$$E_{bv} = \left[r \frac{d\psi_v}{dr} \right]_{r_b^+}, \quad (20)$$

$$E_{vv} = \left[r \frac{d\psi_v}{dr} \right]_{r_v^-}^{r_v^+}. \quad (21)$$

Given that $\psi_s(r)$, $\psi_b(r)$, and $\psi_v(r)$ all individually satisfy Eq. (7), it is easily demonstrated that^{6,18}

$$E_{bs} = E_{sb}, \quad (22)$$

$$E_{vb} = E_{bv}. \quad (23)$$

In fact, it can be shown that

$$E_{vv} = - \frac{2m}{1 - (r_b/r_v)^{2m}}, \quad (24)$$

$$E_{vb} = E_{bv} = \frac{2m (r_b/r_v)^m}{1 - (r_b/r_v)^{2m}}. \quad (25)$$

Equations (10)–(21) yield the asymptotic matching constraints,^{6,18}

$$\Delta\Psi_s = E_{ss} \Psi_s + E_{sb} \Psi_b, \quad (26)$$

$$\Delta\Psi_b = E_{bs} \Psi_s + E_{bb} \Psi_b + E_{bv} \Psi_v, \quad (27)$$

$$\Delta\Psi_v = E_{vb} \Psi_b + E_{vv} \Psi_v. \quad (28)$$

E. Electromagnetic torques

The flux-surface integrated poloidal and toroidal electromagnetic torque densities acting on the plasma can be written as

$$T_\theta(r) = \{r \mathbf{j} \times \mathbf{B} \cdot \mathbf{e}_\theta\}, \quad (29)$$

$$T_\varphi(r) = \{R_0 \mathbf{j} \times \mathbf{B} \cdot \mathbf{e}_z\}, \quad (30)$$

respectively, where

$$\{\dots\} \equiv \oint \oint r R_0 \dots d\theta d\varphi, \quad (31)$$

is a flux-surface integration operator. However, both the plasma equilibrium and the tearing perturbation satisfy the force balance criterion $\mathbf{j} \times \mathbf{B} \simeq \nabla p$. Given that the scalar pressure is a single-valued function of θ and φ , it immediately follows that $T_\theta = T_\varphi = 0$ throughout the plasma.⁶ The only exception to this rule occurs in the immediate vicinity of the rational surface, where Eq. (7) breaks down. It follows that we can write:

$$T_\theta(r) = T_{\theta s} \delta(r - r_s), \tag{32}$$

$$T_\varphi(r) = T_{\varphi s} \delta(r - r_s), \tag{33}$$

where

$$T_{\theta s} = \frac{1}{4} \int_{r_s^-}^{r_s^+} \oint \oint R_0 r^2 (\delta j_\varphi \delta B_r^* + \delta j_\varphi^* \delta B_r - \delta j_r \delta B_\varphi^* - \delta j_r^* \delta B_\varphi) dr d\theta d\varphi, \tag{34}$$

$$T_{\varphi s} = \frac{1}{4} \int_{r_s^-}^{r_s^+} \oint \oint R_0^2 r (\delta j_r \delta B_\theta^* + \delta j_r^* \delta B_\theta - \delta j_\theta \delta B_r^* - \delta j_\theta^* \delta B_r) dr d\theta d\varphi, \tag{35}$$

are the net poloidal and toroidal torques, respectively, acting at the rational surface. Note that the zeroth-order (in perturbed quantities) torques are zero because $B_r = j_r = 0$. Furthermore, the linear (in perturbed quantities) torques average to zero over the flux-surface. Hence, the largest non-zero torques are quadratic in perturbed quantities.

Now, it follows from Eqs. (1)–(6) that:

$$\frac{\delta j_\varphi \delta B_r^* + \delta j_\varphi^* \delta B_r - \delta j_r \delta B_\varphi^* - \delta j_r^* \delta B_\varphi}{(R_0 B_\varphi)^2} \simeq \frac{im}{\mu_0 r^2} \frac{\partial}{\partial r} \left(r \frac{\partial \psi}{\partial r} \psi^* - r \frac{\partial \psi^*}{\partial r} \psi \right), \tag{36}$$

$$\frac{\delta j_r \delta B_\theta^* + \delta j_r^* \delta B_\theta - \delta j_\theta \delta B_r^* - \delta j_\theta^* \delta B_r}{(R_0 B_\varphi)^2} \simeq -\frac{in}{\mu_0 r R_0} \frac{\partial}{\partial r} \left(r \frac{\partial \psi}{\partial r} \psi^* - r \frac{\partial \psi^*}{\partial r} \psi \right). \tag{37}$$

The previous four equations yield^{6,18}

$$T_{\theta s} = -\frac{2\pi^2 R_0^3 B_\varphi^2 m}{\mu_0} \text{Im}(\Delta \Psi_s \Psi_s^*), \tag{38}$$

$$T_{\varphi s} = \frac{2\pi^2 R_0^3 B_\varphi^2 n}{\mu_0} \text{Im}(\Delta \Psi_s \Psi_s^*), \tag{39}$$

where Eqs. (8) and (9) are used.

By analogy with the previous analysis, the poloidal and toroidal electromagnetic torques acting on the inner wall are

$$T_{\theta b} = -\frac{2\pi^2 R_0^3 B_\varphi^2 m}{\mu_0} \text{Im}(\Delta \Psi_b \Psi_b^*), \tag{40}$$

$$T_{\varphi b} = \frac{2\pi^2 R_0^3 B_\varphi^2 n}{\mu_0} \text{Im}(\Delta \Psi_b \Psi_b^*), \tag{41}$$

respectively. Likewise, the poloidal and toroidal electromagnetic torques acting on the outer wall are

$$T_{\theta v} = -\frac{2\pi^2 R_0^3 B_\varphi^2 m}{\mu_0} \text{Im}(\Delta \Psi_v \Psi_v^*), \tag{42}$$

$$T_{\varphi v} = \frac{2\pi^2 R_0^3 B_\varphi^2 n}{\mu_0} \text{Im}(\Delta \Psi_v \Psi_v^*), \tag{43}$$

respectively.

Finally, it is easily demonstrated from Eqs. (22), (23), (26)–(28), and (38)–(43) that^{6,18}

$$T_{\theta s} + T_{\theta b} + T_{\theta v} = 0, \tag{44}$$

$$T_{\varphi s} + T_{\varphi b} + T_{\varphi v} = 0. \tag{45}$$

In other words, the plasma/inner wall/outer wall system cannot exert a net poloidal electromagnetic torque, or a net toroidal electromagnetic torque, on itself.

F. Wall response indices

It is helpful to define the complex dimensionless wall response indices,

$$G_b(t) = \frac{\Delta \Psi_b}{\Psi_b}, \tag{46}$$

$$G_v(t) = \frac{\Delta \Psi_v}{\Psi_v}. \tag{47}$$

Here, G_b specifies the relationship between the eddy current excited in the inner wall and the perturbed magnetic flux that penetrates the wall. Likewise, G_v specifies the analogous relationship for the outer wall. It follows from Eqs. (27) and (28) that:

$$\Psi_b = \frac{E_{bs}}{(-\tilde{E}_{bb})} \frac{\mathcal{G}_v}{(\mathcal{G}_b + \Gamma_{bv}) \mathcal{G}_v - \Gamma_{bv}} \Psi_s, \tag{48}$$

$$\Psi_v = \frac{E_{bs}}{E_{bv}} \frac{\Gamma_{bv}}{(\mathcal{G}_b + \Gamma_{bv}) \mathcal{G}_v - \Gamma_{bv}} \Psi_s, \tag{49}$$

where

$$\mathcal{G}_b = 1 + \frac{G_b}{(-\tilde{E}_{bb})}, \tag{50}$$

$$\mathcal{G}_v = 1 + \frac{G_v}{(-E_{vv})}, \tag{51}$$

$$\tilde{E}_{bb} = E_{bb} - \frac{E_{bv} E_{vb}}{E_{vv}}, \tag{52}$$

$$\Gamma_{bv} = -1 + \frac{E_{bb}}{\tilde{E}_{bb}} = \frac{2m(r_b/r_v)^{2m}}{1 - (r_b/r_v)^{2m}} \frac{1}{(-\tilde{E}_{bb})}. \tag{53}$$

Finally, Eqs. (26) and (48) yield

$$\frac{\Delta \Psi_s}{\Psi_s} = \Delta_{pw} + (\Delta_{nw} - \Delta_{pw}) \mathcal{G}_{bv}, \tag{54}$$

where

$$\Delta_{pw} = E_{ss}, \tag{55}$$

$$\Delta_{nw} = E_{ss} + \frac{E_{sb} E_{bs}}{(-\tilde{E}_{bb})}, \tag{56}$$

$$\mathcal{G}_{bv} = \frac{\mathcal{G}_v}{(\mathcal{G}_b + \Gamma_{bv}) \mathcal{G}_v - \Gamma_{bv}}. \tag{57}$$

Here, Δ_{pw} is the (dimensionless) tearing stability index¹⁶ when the inner wall is perfectly conducting, whereas Δ_{nw} is the tearing stability index when there are no walls surrounding the plasma.

G. Island width evolution

The reconnected magnetic flux at the rational surface generates a helical magnetic island chain whose full radial width is

$$W = 4 (L_s R_0 |\Psi_s|)^{1/2}. \tag{58}$$

Here, $L_s = R_0 q_s/s_s$ is the magnetic shear-length at the rational surface. Moreover, $q_s = q(r_s) = m/n$, $s_s = s(r_s)$, and $s(r) = r q'/q$. The width of the magnetic island chain evolves in time according to the Rutherford island width evolution equation,¹⁹

$$I_1 \tau_R \frac{d}{dt} \left(\frac{W}{r_s} \right) = \text{Re} \left(\frac{\Delta \Psi_s}{\Psi_s} \right), \tag{59}$$

where $I_1 = 0.8227$, and $\tau_R = \mu_0 r_s^2/\eta_{\parallel}(r_s)$ is the resistive evolution time at the rational surface. Here, $\eta_{\parallel}(r)$ is the plasma electrical resistivity profile. It follows from Eq. (54) that:

$$I_1 \tau_R \frac{d}{dt} \left(\frac{W}{r_s} \right) = \Delta_{pw} + (\Delta_{nw} - \Delta_{pw}) \text{Re}(\mathcal{G}_{bv}). \tag{60}$$

According to the standard neoclassical theory (assuming that the plasma at the rational surface lies in the banana collisionality regime),²⁰⁻²²

$$\eta_{\parallel} = Q_{11}^{ee} \frac{n_e e^2 \tau_e}{m_e}, \tag{61}$$

where n_e is the electron number density, τ_e is the electron collision time,²³ m_e is the electron mass, and

$$[Q^{ee}] = \begin{bmatrix} F_{11}^{ee} + \mu_{11}^e & F_{12}^{ee} + \mu_{12}^e \\ F_{12}^{ee} + \mu_{12}^e & F_{22}^{ee} + \mu_{22}^e \end{bmatrix}^{-1}, \tag{62}$$

$$F_{11}^{ee} = Z_{\text{eff}}, \tag{63}$$

$$F_{12}^{ee} = \frac{3}{2} Z_{\text{eff}}, \tag{64}$$

$$F_{22}^{ee} = \sqrt{2} + \frac{13}{4} Z_{\text{eff}}, \tag{65}$$

$$\mu_{11}^e = g_t (0.533 + Z_{\text{eff}}), \tag{66}$$

$$\mu_{12}^e = g_t \left(0.625 + \frac{3}{2} Z_{\text{eff}} \right), \tag{67}$$

$$\mu_{22}^e = g_t \left(1.386 + \frac{13}{4} Z_{\text{eff}} \right). \tag{68}$$

Here, $g_t = f_i/(1 - f_i)$, f_i is the fraction of trapped particles, and Z_{eff} is the effective ion charge number.

Note that we have neglected the destabilizing effect of the perturbed bootstrap current in Eq. (60), for the sake of simplicity. This approximation is reasonable because the bootstrap contribution to Δ_{pw} is similar in magnitude to the classical contribution.¹⁴ We have, however, attempted to make as accurate an estimate as possible of the parallel plasma resistivity, taking impurities and neoclassical effects into account, because it is important that our estimate for the

neoclassical resistivity be consistent with our estimate for the neoclassical poloidal flow-damping rate.

Equation (60) implies that, in the presence of a perfectly conducting inner wall (i.e., $\mathcal{G}_{bv} = 0$), the island width grows without limit if $\Delta_{pw} > 0$. In fact, this is not the case. If the asymptotic matching at the rational surface is carried out to higher order, then this equation becomes²⁴

$$I_1 \tau_R \frac{d}{dt} \left(\frac{W}{r_s} \right) = \Delta_{pw}(0) \left(1 - \frac{W}{W_{pw}} \right) + [\Delta_{nw}(0) - \Delta_{pw}(0)] \text{Re}(\mathcal{G}_{bv}), \tag{69}$$

where

$$W_{pw} = \frac{\Delta_{pw}(0) r_s}{0.8 \alpha_s^2 - 0.27 \beta_s - 0.09 \alpha_s}, \tag{70}$$

$$\alpha_s = - \left(\frac{r q J'_{\phi}}{s} \right)_{r_s}, \tag{71}$$

$$\beta_s = - \left(\frac{r q J''_{\phi}}{s} \right)_{r_s}. \tag{72}$$

Here, $\Delta_{pw}(0)$ denotes the perfect-wall tearing stability index evaluated at zero island width. Likewise, $\Delta_{nw}(0)$ denotes the no-wall tearing stability index evaluated at zero island width. Finally, W_{pw} is the saturated island width when the inner wall is perfectly conducting.

H. Island frequency evolution

We can write

$$\Psi_s(t) = \frac{W^2(t)}{16 L_s R_0} \exp \left(-i \int_0^t \omega(t') dt' \right), \tag{73}$$

where $\omega(t)$ is the instantaneous angular rotation frequency of the magnetic island chain. The island rotation frequency evolves in time according to^{6,18}

$$\omega(t) = \omega_0 + m \Delta \Omega_{\theta}(r_s, t) - n \Delta \Omega_{\phi}(r_s, t), \tag{74}$$

where ω_0 is the angular rotation frequency in the absence of the walls, otherwise known as the natural frequency,⁶ whereas $\Delta \Omega_{\theta}(r, t)$ and $\Delta \Omega_{\phi}(r, t)$ are the modifications to the plasma poloidal and toroidal angular velocity profiles, respectively, generated by the electromagnetic torques exerted at the rational surface by the eddy currents excited in the walls.

I. Plasma angular equations of motion

The plasma poloidal equation of angular motion takes the form⁶

$$4\pi^2 R_0 \left[\rho r^3 \frac{\partial \Delta \Omega_{\theta}}{\partial t} + \frac{\rho}{\tau_{\theta}} r^3 \Delta \Omega_{\theta} - \frac{\partial}{\partial r} \left(\rho \Xi_{\perp} r^3 \frac{\partial \Delta \Omega_{\theta}}{\partial r} \right) \right] = T_{0s} \delta(r - r_s). \tag{75}$$

Here, $\rho(r)$ is the plasma mass density profile, $\Xi_{\perp}(r)$ is the perpendicular momentum diffusivity profile, and

$$\tau_{\theta}(r) = \frac{1}{\sqrt{2} \mu_{11}^i g_t} \left(\frac{\epsilon}{q} \right)^2 \tau_i, \tag{76}$$

the neoclassical poloidal flow-damping rate.²² Moreover, $\mu_{11}^i = 0.533 + \alpha_I$,^{20–22} where

$$\alpha_I = \frac{Z_I (Z_{\text{eff}} - 1)}{Z_I - Z_{\text{eff}}}, \quad (77)$$

Z_I is the impurity ion charge number, $\epsilon(r) = r/R_0$, and τ_i is the ion collision time.²³ The plasma toroidal equation of angular motion is written as⁶

$$4\pi^2 R_0^3 \left[\rho r \frac{\partial \Delta \Omega_\varphi}{\partial t} - \frac{\partial}{\partial r} \left(\rho \Xi_\perp r \frac{\partial \Delta \Omega_\varphi}{\partial r} \right) \right] = T_{\varphi s} \delta(r - r_s). \quad (78)$$

Equations (75) and (78) must be solved subject to the boundary conditions

$$\frac{\partial \Delta \Omega_\theta(0, t)}{\partial r} = \frac{\partial \Delta \Omega_\varphi(0, t)}{\partial r} = 0, \quad (79)$$

$$\Delta \Omega_\theta(a, t) = \Delta \Omega_\varphi(a, t) = 0. \quad (80)$$

The boundary conditions (79) merely ensure that the angular velocities remain finite at the magnetic axis. On the other hand, the boundary conditions (80) are a consequence of the action of charge exchange with electrically neutral particles emitted isotropically from the wall in the edge regions of the plasma.⁶

J. Solution of plasma angular equations of motion

During the time interval in which mode locking occurs, the perturbed angular velocity profiles, $\Delta \Omega_\theta(r, t)$ and $\Delta \Omega_\varphi(r, t)$, are localized in the vicinity of the rational surface.⁶ Hence, it is reasonable to express the perturbed angular equations of motion, (75) and (78), in the simplified forms

$$4\pi^2 R_0 \left[\rho_s r^3 \frac{\partial \Delta \Omega_\theta}{\partial t} + \frac{\rho_s}{\tau_{\theta s}} r^3 \Delta \Omega_\theta - \rho_s \Xi_{\perp s} \frac{\partial}{\partial r} \left(r^3 \frac{\partial \Delta \Omega_\theta}{\partial r} \right) \right] = T_{\theta s} \delta(r - r_s), \quad (81)$$

$$4\pi^2 R_0^3 \left[\rho_s r \frac{\partial \Delta \Omega_\varphi}{\partial t} - \rho_s \Xi_{\perp s} \frac{\partial}{\partial r} \left(r \frac{\partial \Delta \Omega_\varphi}{\partial r} \right) \right] = T_{\varphi s} \delta(r - r_s), \quad (82)$$

where $\rho_s = \rho(r_s)$, $\tau_{\theta s} = \tau_\theta(r_s)$, and $\Xi_{\perp s} = \Xi_\perp(r_s)$.

Let us write^{7,25}

$$\Delta \Omega_\theta(r, t) = -\frac{1}{m} \sum_{p=1, \infty} \alpha_p(t) \frac{y_p(r/a)}{y_p(r_s/a)}, \quad (83)$$

$$\Delta \Omega_\varphi(r, t) = \frac{1}{n} \sum_{p=1, \infty} \beta_p(t) \frac{z_p(r/a)}{z_p(r_s/a)}, \quad (84)$$

where $y_p(r) = J_1(j_{1p} r/a)/(r/a)$ and $z_p(r) = J_0(j_{0p} r/a)$. Here, $J_m(z)$ is a Bessel function, and j_{mp} denotes its p th zero. Note that Eqs. (83) and (84) automatically satisfy the boundary conditions (79) and (80).

It is easily demonstrated that

$$\frac{d}{dr} \left(r^3 \frac{dy_p}{dr} \right) = -\frac{j_{1p}^2 r^3 y_p}{a^2}, \quad (85)$$

$$\frac{d}{dr} \left(r \frac{dz_p}{dr} \right) = -\frac{j_{0p}^2 r z_p}{a^2}, \quad (86)$$

and

$$\int_0^a r^3 y_p(r) y_q(r) dr = \frac{a^4}{2} [J_2(j_{1p})]^2 \delta_{pq}, \quad (87)$$

$$\int_0^a r z_p(r) z_q(r) dr = \frac{a^2}{2} [J_1(j_{0p})]^2 \delta_{pq}. \quad (88)$$

Equations (81)–(88) can be combined with Eqs. (38), (39), (58), and (74) to give

$$\omega(t) = \omega_0 - \sum_{p=1, \infty} [\alpha_p(t) + \beta_p(t)], \quad (89)$$

where

$$\tau_M \frac{d\alpha_p}{dt} + (\zeta_\theta + j_{1p}^2) \alpha_p = g_{\theta p} \left(\frac{\tau_\varphi}{\tau_{\theta H}^2} \right) \left(\frac{w}{r_s} \right)^4 \text{Im} \left(\frac{\Delta \Psi_s}{\Psi_s} \right), \quad (90)$$

$$\tau_M \frac{d\beta_p}{dt} + j_{0p}^2 \beta_p = g_{\varphi p} \left(\frac{\epsilon_s}{q_s} \right)^2 \left(\frac{\tau_\varphi}{\tau_{\theta H}^2} \right) \left(\frac{w}{r_s} \right)^4 \text{Im} \left(\frac{\Delta \Psi_s}{\Psi_s} \right), \quad (91)$$

and $\tau_M = a^2/\Xi_{\perp s}$, $\tau_\varphi = r_s^2/\Xi_{\perp s}$,

$$\tau_H = \frac{L_s (\mu_0 \rho_s)^{1/2}}{m B_\varphi}, \quad (92)$$

$$\zeta_\theta = \frac{\tau_M}{\tau_{\theta s}}, \quad (93)$$

$$g_{\theta p} = \left[\frac{J_1(j_{1p} r_s/a)}{J_2(j_{1p})} \right]^2, \quad (94)$$

$$g_{\varphi p} = \left[\frac{J_0(j_{0p} r_s/a)}{J_1(j_{0p})} \right]^2, \quad (95)$$

$w = W/4$, and $\epsilon_s = \epsilon(r_s)$.

K. Wall physics

Suppose that the inner wall extends from $r = r_b$ to $r = r_b + \delta_b$, where $\delta_b \ll r_b$ is the wall thickness. Ohm's law inside the wall yields

$$\frac{\partial^2 \psi}{\partial r^2} \simeq \frac{\mu_0}{\eta_b} \frac{\partial \psi}{\partial t}, \quad (96)$$

where η_b is the electrical resistivity of the inner wall material. The previous equation must be solved subject to the boundary conditions,

$$\psi(r_b, t) = \Psi_b(t), \quad (97)$$

$$\frac{\partial \ln \psi(r_b + \delta_b, t)}{\partial \ln r} = -m_b, \quad (98)$$

where

$$m_b = m \left\{ \frac{\mathcal{G}_v + (\mathcal{G}_v - 2) (r_b/r_v)^{2m}}{\mathcal{G}_v [1 - (r_b/r_v)^{2m}]} \right\}. \quad (99)$$

These boundary conditions follow from Eqs. (7), (14), (48), (49), and (53). Note that we have effectively redefined Ψ_b to be the normalized helical magnetic flux that penetrates the inner (in r) boundary of the inner wall.

Let

$$\rho = \frac{r - r_b}{\delta_b}, \quad (100)$$

$$\psi(r, t) = \Psi_b(t) F(\rho). \tag{101}$$

Equations (96)–(98) yield

$$\frac{\partial^2 F}{\partial \rho^2} = \tau_b \zeta_b \gamma_b F, \tag{102}$$

$$F(0) = 1, \tag{103}$$

$$\frac{\partial \ln F(1)}{\partial \rho} \simeq -m_b \zeta_b, \tag{104}$$

where

$$\gamma_b = \frac{d \ln \Psi_b}{dt}, \tag{105}$$

$$\tau_b = \frac{\mu_0 r_b \delta_b}{\eta_b}, \tag{106}$$

$$\zeta_b = \frac{\delta_b}{r_b}. \tag{107}$$

Here, τ_b is the time-constant of the inner wall.^{4,15} Note that, in writing Eq. (102), we have neglected transient eddy currents excited in the inner wall, for the sake of simplicity. (See Ref. 7 for an explanation of how transient eddy currents could be incorporated into the analysis.)

Equations (102)–(104) can be solved to give

$$F(\rho) = \frac{\alpha_b \cosh[\alpha_b(\rho - 1)] - m_b \zeta_b \sinh[\alpha_b(\rho - 1)]}{\alpha_b \cosh \alpha_b + m_b \zeta_b \sinh \alpha_b}, \tag{108}$$

where

$$\alpha_b = \sqrt{\gamma_b \tau_b \zeta_b}. \tag{109}$$

However, in the physically relevant limit,

$$m_b^2 \zeta_b \ll |\gamma_b| \tau_b, \tag{110}$$

expression (108) simplifies to

$$F(\rho) \simeq \frac{\cosh[\alpha_b(\rho - 1)]}{\cosh \alpha_b}. \tag{111}$$

Equation (11) generalizes to give

$$\Delta \Psi_b = \left[r \frac{\partial \psi}{\partial r} \right]_{r_b}^{r_b + \delta_b} \simeq \frac{\Psi_b}{\zeta_b} \left[\frac{\partial F}{\partial \rho} \right]_0^1, \tag{112}$$

where Eqs. (100), (101), and (107) have been used. It follows from Eqs. (46), (109), and (111) that the wall response index for the inner wall takes the form:

$$G_b = \sqrt{\frac{\gamma_b \tau_b}{\zeta_b}} \tanh\left(\sqrt{\gamma_b \tau_b \zeta_b}\right). \tag{113}$$

In the so-called thin-wall limit,

$$m_b^2 \zeta_b \ll |\gamma| \tau_b \ll \frac{1}{\zeta_b}, \tag{114}$$

in which the thickness of the wall is much less than the skin-depth, the wall response index reduces to the standard form^{4,15}

$$G_b \simeq \gamma_b \tau_b. \tag{115}$$

On the other hand, in the thick-wall limit,

$$\frac{1}{\zeta_b} \ll |\gamma_b| \tau_b, \tag{116}$$

in which the thickness of the wall is much greater than the skin-depth, we obtain^{1,15}

$$G_b \simeq \sqrt{\frac{\gamma_b \tau_b}{\zeta_b}}. \tag{117}$$

The previous expression represents a wall response in which the eddy current only penetrates a distance of order the skin-depth into the wall from its inner boundary.

By analogy with Eq. (113), the wall response index for the outer wall takes the form

$$G_v = \sqrt{\frac{\gamma_v \tau_v}{\zeta_v}} \tanh\left(\sqrt{\gamma_v \tau_v \zeta_v}\right), \tag{118}$$

where

$$\gamma_v = \frac{d \ln \Psi_v}{dt}, \tag{119}$$

$$\tau_v = \frac{\mu_0 r_v \delta_v}{\eta_v}, \tag{120}$$

$$\zeta_v = \frac{\delta_v}{r_v}. \tag{121}$$

Here, δ_v , η_v , and τ_v are the thickness, electrical resistivity, and time-constant of the outer wall, respectively.

Equations (50), (51), (113), and (118) yield

$$\mathcal{G}_b = 1 + \sqrt{\frac{\gamma_b \tilde{\tau}_b}{\tilde{\zeta}_b}} \tanh\left(\sqrt{\gamma_b \tilde{\tau}_b \tilde{\zeta}_b}\right), \tag{122}$$

$$\mathcal{G}_v = 1 + \sqrt{\frac{\gamma_v \tilde{\tau}_v}{\tilde{\zeta}_v}} \tanh\left(\sqrt{\gamma_v \tilde{\tau}_v \tilde{\zeta}_v}\right), \tag{123}$$

where

$$\tilde{\tau}_b = \frac{\tau_b}{(-\tilde{E}_{bb})}, \tag{124}$$

$$\tilde{\zeta}_b = \frac{\delta_b}{r_b} (-\tilde{E}_{bb}), \tag{125}$$

$$\tilde{\tau}_v = \frac{\tau_v}{(-E_{vv})}, \tag{126}$$

$$\tilde{\zeta}_v = \frac{\delta_v}{r_v} (-E_{vv}). \tag{127}$$

Finally, Eqs. (48), (49), (73), (105), (119), (122), and (123) give

$$\mathcal{H}_b \frac{d\gamma_b}{dt} = (G_b + \Gamma_{bv})(\gamma_v - \gamma_b) + \frac{1}{G_{bv}}(\gamma - \gamma_v), \tag{128}$$

$$\mathcal{H}_v \frac{d\gamma_v}{dt} = \mathcal{G}_v(\gamma_b - \gamma_v), \tag{129}$$

where

$$\gamma \equiv \frac{d \ln \Psi_s}{dt} = 2 \frac{d \ln W}{dt} - i \omega, \quad (130)$$

$$\mathcal{H}_b = \frac{1}{2} \left[\sqrt{\frac{\tilde{\tau}_b}{\gamma_b \tilde{\zeta}_b}} \tanh \left(\sqrt{\gamma_b \tilde{\tau}_b \tilde{\zeta}_b} \right) + \frac{\tilde{\tau}_b}{\cosh^2 \left(\sqrt{\gamma_b \tilde{\tau}_b \tilde{\zeta}_b} \right)} \right], \quad (131)$$

$$\mathcal{H}_v = \frac{1}{2} \left[\sqrt{\frac{\tilde{\tau}_v}{\gamma_v \tilde{\zeta}_v}} \tanh \left(\sqrt{\gamma_v \tilde{\tau}_v \tilde{\zeta}_v} \right) + \frac{\tilde{\tau}_v}{\cosh^2 \left(\sqrt{\gamma_v \tilde{\tau}_v \tilde{\zeta}_v} \right)} \right]. \quad (132)$$

L. Normalized rotation braking equations

Let $x = w/w_{pw}$, $y = \omega/\omega_0$, and $T = t \omega_0$. Here, $w_{pw} = W_{pw}/4$. Thus, x is the width of the magnetic island chain relative to its saturated width when the inner wall is perfectly conducting, y is the island rotation frequency relative to the natural frequency, and T is time normalized to the typical time required for the island chain complete a full rotation. Equations (57), (69), (89)–(91), (122), (123), and (128)–(132) reduce to the following closed set of equations that determine the time evolution of the normalized island rotation frequency:

$$y(T) = 1 - \sum_{p=1, \infty} \left[\hat{\alpha}_p(T) + \hat{\beta}_p(T) \right], \quad (133)$$

where

$$\hat{\tau}_M \frac{d \hat{\alpha}_p}{dT} = - \left(\zeta_\theta + j_{1p}^2 \right) \hat{\alpha}_p + g_{\theta p} \Gamma_\theta x^4 \text{Im}(\mathcal{G}_{bv}), \quad (134)$$

$$\hat{\tau}_M \frac{d \hat{\beta}_p}{dT} = -j_{0p}^2 \hat{\beta}_p + g_{\phi p} \Gamma_\phi x^4 \text{Im}(\mathcal{G}_{bv}), \quad (135)$$

$$\hat{\tau}_{pw} \frac{dx}{dT} = 1 - x + \Gamma_x \text{Re}(\mathcal{G}_{bv}), \quad (136)$$

and

$$\mathcal{G}_{bv} = \frac{\mathcal{G}_v}{(\mathcal{G}_b + \Gamma_{bv}) \mathcal{G}_v - \Gamma_{bv}}, \quad (137)$$

$$\mathcal{G}_b = 1 + \sqrt{\frac{\hat{\gamma}_b \tilde{\tau}_b}{\tilde{\zeta}_b}} \tanh \left(\sqrt{\hat{\gamma}_b \tilde{\tau}_b \tilde{\zeta}_b} \right), \quad (138)$$

$$\mathcal{G}_v = 1 + \sqrt{\frac{\hat{\gamma}_v \tilde{\tau}_v}{\tilde{\zeta}_v}} \tanh \left(\sqrt{\hat{\gamma}_v \tilde{\tau}_v \tilde{\zeta}_v} \right), \quad (139)$$

with

$$\mathcal{H}_b \frac{d \hat{\gamma}_b}{dT} = (\mathcal{G}_b + \Gamma_{bv}) (\hat{\gamma}_v - \hat{\gamma}_b) + \frac{1}{\mathcal{G}_{bv}} (\hat{\gamma} - \hat{\gamma}_v), \quad (140)$$

$$\mathcal{H}_v \frac{d \hat{\gamma}_v}{dT} = \mathcal{G}_v (\hat{\gamma}_b - \hat{\gamma}_v), \quad (141)$$

where

$$\hat{\gamma} = 2 \frac{d \ln x}{dT} - i y, \quad (142)$$

$$\mathcal{H}_b = \frac{1}{2} \left[\sqrt{\frac{\hat{\tau}_b}{\hat{\gamma}_b \tilde{\zeta}_b}} \tanh \left(\sqrt{\hat{\gamma}_b \tilde{\tau}_b \tilde{\zeta}_b} \right) + \frac{\hat{\tau}_b}{\cosh^2 \left(\sqrt{\hat{\gamma}_b \tilde{\tau}_b \tilde{\zeta}_b} \right)} \right], \quad (143)$$

$$\mathcal{H}_v = \frac{1}{2} \left[\sqrt{\frac{\hat{\tau}_v}{\hat{\gamma}_v \tilde{\zeta}_v}} \tanh \left(\sqrt{\hat{\gamma}_v \tilde{\tau}_v \tilde{\zeta}_v} \right) + \frac{\hat{\tau}_v}{\cosh^2 \left(\sqrt{\hat{\gamma}_v \tilde{\tau}_v \tilde{\zeta}_v} \right)} \right]. \quad (144)$$

Here, Γ_{bv} , ζ_θ , $g_{\theta p}$, $g_{\phi p}$, $\tilde{\zeta}_b$, and $\tilde{\zeta}_v$ are defined in Eqs. (53), (93), (94), (95), (125), and (127), respectively. Moreover,

$$\hat{\tau}_M = \tau_M \omega_0, \quad (145)$$

$$\hat{\tau}_{pw} = \tau_{pw} \omega_0, \quad (146)$$

$$\tau_{pw} = \frac{I_1 \tau_R}{\Delta_{pw}(0)} \frac{W_{pw}}{r_s}, \quad (147)$$

$$\hat{\tau}_b = \frac{\tau_b \omega_0}{(-\tilde{E}_{bb})}, \quad (148)$$

$$\hat{\tau}_v = \frac{\tau_v \omega_0}{(-E_{vv})}, \quad (149)$$

$$\Gamma_\theta = [\Delta_{nw}(0) - \Delta_{pw}(0)] \left(\frac{\tau_\phi}{\tau_H^2 \omega_0} \right) \left(\frac{w_{pw}}{r_s} \right)^4, \quad (150)$$

$$\Gamma_\phi = \left(\frac{\epsilon_s}{q_s} \right)^2 \Gamma_\theta, \quad (151)$$

$$\Gamma_x = \frac{\Delta_{nw}(0) - \Delta_{pw}(0)}{\Delta_{pw}(0)}. \quad (152)$$

Note that τ_{pw} is the typical time required for the island chain to attain its final saturated width.

M. Approximation

If we neglect plasma inertia (i.e., the terms involving d/dT), then Eqs. (133)–(135) yield

$$\mathcal{T}(T) \equiv y + \Gamma_{\theta\phi} x^4 \text{Im}(\mathcal{G}_{bv}) - 1 = 0, \quad (153)$$

where

$$\Gamma_{\theta\phi} = \frac{1}{4} \left[\left(\frac{\tau_{\theta s}}{\tau_\phi} \right)^{1/2} \Gamma_\theta + 2 \ln \left(\frac{a}{r_s} \right) \Gamma_\phi \right]. \quad (154)$$

Here, the results have been used,²⁶

$$\lim_{\epsilon \rightarrow 0} \sum_{p=1, \infty} \frac{\sqrt{\epsilon} [J_1(j_{1p} x)]^2}{[J_2(j_{1p})]^2 (1 + \epsilon j_{1p}^2)} \simeq \frac{1}{4x}, \quad (155)$$

$$\sum_{p=1, \infty} \frac{[J_0(j_{0p} x)]^2}{[J_1(j_{0p})]^2 j_{0p}^2} = \frac{1}{2} \ln \left(\frac{1}{x} \right). \quad (156)$$

Unfortunately, when the summations in the previous two expressions are truncated, as they must be in practice, the first expression is found to converge to its final value comparatively slowly. In order to avoid retaining an unpractical number of velocity harmonics in the calculation, Eq. (133) is replaced by

$$y = 1 - \frac{1}{S_\theta} \sum_{p=1, p_{\theta \max}} \hat{\alpha}_p - \frac{1}{S_\phi} \sum_{p=1, p_{\phi \max}} \hat{\beta}_p, \quad (157)$$

where

$$S_\theta = 4 \left(\frac{r_s}{a} \right) \sqrt{\zeta_\theta} \sum_{p=1, p_{\theta \max}} \frac{g_{\theta p}}{\zeta_\theta + J_{1p}^2}, \quad (158)$$

$$S_\phi = \frac{2}{\ln(a/r_s)} \sum_{p=1, p_{\phi \max}} \frac{g_{\phi p}}{J_{0p}^2}. \quad (159)$$

Note that $S_\theta \rightarrow 1$ as $p_{\theta \max} \rightarrow \infty$, and $S_\phi \rightarrow 1$ as $p_{\phi \max} \rightarrow \infty$. With these changes, \mathcal{T} , which is defined in Eq. (153), becomes an accurate torque balance diagnostic. In other words, $\mathcal{T} \simeq 0$ when the plasma is in a torque-balanced state (i.e., a state in which the electromagnetic torque at the rational surface is exactly balanced by the viscous and poloidal flow-damping torques), and plasma inertia is not playing a role in determining the angular velocity profiles, whereas $\mathcal{T} \sim \mathcal{O}(1)$ when torque balance breaks down.

In conclusion, our final set of rotation braking equations are Eqs. (134)–(144) and (157). These equations are integrated using an explicit, adaptive step, embedded Runge–Kutta Cash–Karp (4, 5) method.

III. LOCKING OF 2/1 TEARING MODE IN ITER

A. Simulation parameters

Like La Haye *et al.*,¹⁴ we shall consider locking of the 2/1 tearing mode in the ITER 15 MA inductive scenario 2.²⁷ Plasma profiles for this scenario obtained by Urso²⁸ originate from simulations by Polevoi *et al.*²⁹

The main plasma parameters are $B_\phi = 5.3$ T, $R_0 = 5.3$ m, $a = 2.0$ m, $Z_{\text{eff}} = 1.7$, $Z_I = 4$ (beryllium), and $\tau_M = 3.7$ s.^{28,29} The $m = 2/n = 1$ rational surface lies at $r_s/a = 0.87$.^{28,29} The electron number density, electron temperature, ion temperature, neoclassical plasma resistivity, and natural frequency at this surface are $n_e = 9.8 \times 10^{19} \text{ m}^{-3}$, $T_e = 5.6$ keV, $T_i = 5.7$ keV, $\eta_{\parallel} = 3.4 \times 10^{-8} \Omega \text{ m}$, and $\omega_0 = 0.42$ kHz, respectively.^{28,29}

In our study, we shall use a “Wesson”-type plasma current density profile of the form $J_\phi = J_\phi(0) (1 - r^2/a^2)^\nu$, where $q(a) = 2/J_\phi(0)$ and $q(0) = q(a)/(1 + \nu)$.¹⁷ The choices $q(0) = 0.8$ and $q(a) = 2.6$ yield $r_s/a = 0.87$. [Note that the rather low value for $q(a)$ is an artifact of using a cylindrical model to describe a toroidal plasma. The $q(a)$ value is chosen so as to ensure that the 2/1 rational surface lies at the same minor radius as in the La Haye study.] The choice $f_i = 0.91$ is consistent with $\eta_{\parallel} = 3.4 \times 10^{-8} \Omega \text{ m}$.

Finally, our adopted wall parameters are $r_b = 1.2 a$, $\delta_b = 0.25 a$, $\tau_b = 23$ ms, $r_v = 1.5 a$, $\tau_v = 0.369$ s, and $\eta_v = 7.4 \times 10^{-7} \Omega \text{ m}$ (see Sec. I.). Note that we are assuming that the blanket module layer fills most of the space between its inner surface and the inner surface of the vacuum vessel. The effective electrical resistivity of the blanket module layer is $6.6 \times 10^{-5} \Omega \text{ m}$. The effective thickness of the vacuum vessel is $\delta_b = 7.4$ cm.

We find that $\Delta_{pw}(0) = 2.49$, $\Delta_{nw}(0) = 3.79$, $W_{pw} = 0.45 a$, $\tilde{E}_{bb} = -5.60$, and $\tilde{E}_{vv} = -6.78$. The various timescales in the calculation are $\tau_H = 4.2 \times 10^{-7}$, $\tau_{\theta s} = 6.4 \times 10^{-6}$, $\tau_M = 3.7$, and $\tau_{pw} = 19$ s.

The normalized simulation parameters are $\tilde{\zeta}_b = 1.17$, $\tilde{\zeta}_v = 0.17$, $\tilde{\zeta}_\theta = 5.8 \times 10^5$, $\hat{\tau}_b = 10.8$, $\hat{\tau}_v = 1.5 \times 10^2$, $\hat{\tau}_M = 9.8 \times 10^3$, $\hat{\tau}_{pw} = 5.0 \times 10^4$, $\Gamma_\theta = 2.1 \times 10^6$, $\Gamma_\phi = 4.2 \times 10^4$, $\Gamma_x = 0.52$, $\Gamma_{\theta\phi} = 3.7 \times 10^3$, and $\Gamma_{bv} = 0.50$.

The number of poloidal velocity harmonics retained in the calculation is $p_{\theta \max} = 500$, while the number of toroidal velocity harmonics retained in the calculation is $p_{\phi \max} = 100$.

B. Simulation results

Figure 1 shows the 2/1 island width and island angular frequency calculated as functions of time using our model. Figure 2 shows the same parameters in unnormalized units. It can be seen that the 2/1 tearing mode locks to the walls when it has attained about 20% of its final saturated width. Looking more closely, it is clear that the mode locks to the walls in two stages. First, it locks to the blanket module layer and is left rotating at about 15 Hz. Next, it locks to the vacuum vessel and is left rotating at less than 0.5 Hz. The time required for the 2/1 mode to grow from a small amplitude and lock to the blanket module layer is 3.6 s, whereas that required to lock to the vacuum vessel is 3.9 s. The island width when the mode locks to the blanket module layer is 8.9% of the plasma minor radius, whereas that when the mode locks to the vacuum vessel is 9.6%. The figures also show the results of a “thin-wall” calculation in which the time constants of the inner and outer wall are kept the same as in the thick-wall calculation, but the dimensionless wall thickness parameters, $\tilde{\zeta}_b$ and $\tilde{\zeta}_v$, are both given very small values. It can be seen that the thin-wall slowing down curve is a little different from its thick-wall counterpart. On the other hand, the critical island width at which the mode locks to the wall is the same in both cases.

According to our calculation, the time required for the 2/1 tearing mode to grow from a small amplitude to one large enough to lock to the walls is about 50% larger than that reported by La Haye *et al.*¹⁴ On the other hand, the critical island width at which wall locking occurs is about twice that reported by La Haye *et al.* This finding is significant because a critical island width for wall locking in ITER of about 9% is similar to that seen in existing (large) tokamaks.¹⁴

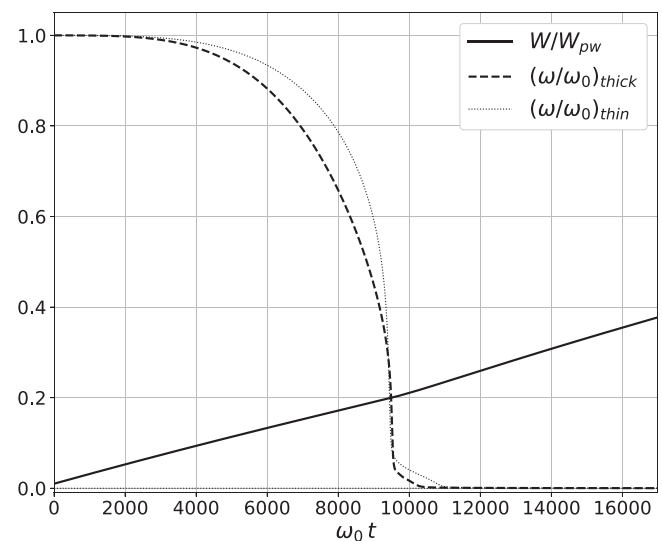


FIG. 1. Island width and island angular rotation frequency as functions of time for a growing 2/1 tearing mode in ITER. Here, $W_{pw} = 90$ cm, and $\omega_0 = 0.42$ kHz. The subscripts “thick” and thin indicate thin-wall and thick-wall calculations, respectively.

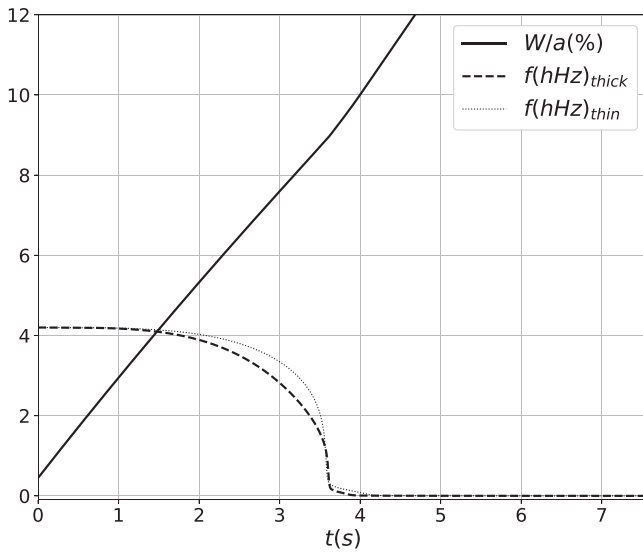


FIG. 2. Island width and island rotation frequency as functions of time for a growing 2/1 tearing mode in ITER. The subscripts thick and thin indicate thin-wall and thick-wall calculations, respectively.

Figure 3 shows the fractions of the 2/1 tearing mode frequency shift that is due to changes in the plasma poloidal and toroidal angular velocities at the rational surface as functions of time. It can be seen that about 22% of the mode frequency shift associated with wall locking is due to changes in the plasma poloidal angular velocity, the remaining 78% being due to changes in the plasma toroidal angular velocity. Clearly, it is not the case that neoclassical poloidal flow-damping is strong enough to completely suppress plasma poloidal

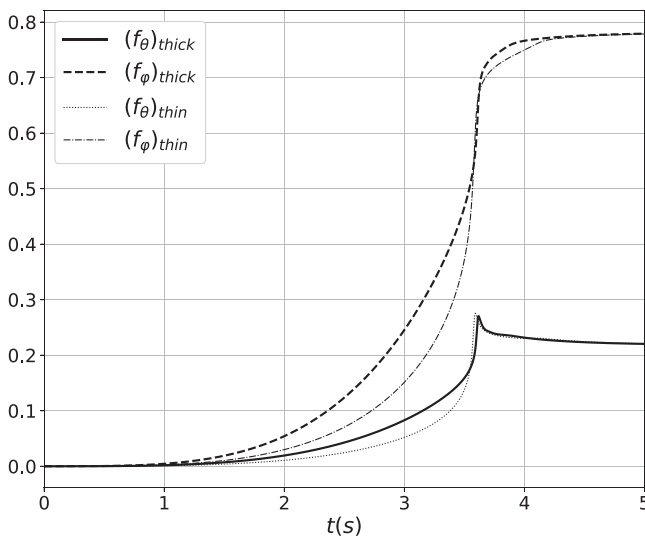


FIG. 3. Fraction of 2/1 mode frequency shift that is due to changes in the plasma poloidal (f_θ) and toroidal (f_ϕ) angular velocities at the rational surface as functions of time. The subscripts thick and thin indicate thin-wall and thick-wall calculations, respectively.

angular velocity shifts associated with mode locking in ITER (or in any existing tokamak). Note that the poloidal angular velocity shift during the time interval in which the mode frequency collapses evolves on a significantly shorter timescale than the toroidal angular velocity shift. The figure also shows the results of a thin-wall calculation. It can be seen that the thin-wall frequency shift curves are a slightly different than the thick-wall curves.

Figure 4 shows the fractions of the reconnected magnetic flux that penetrate the blanket module layer and the vacuum vessel as functions of time. It can be seen that the magnetic flux penetrates the walls in two stages. First, it penetrates the blanket module layer over a timescale of about 50 ms. Next, it penetrates the vacuum vessel over a timescale of about 500 ms. Note that, even when the mode rotation is not significantly slowed, the reconnected flux still partially penetrates both the blanket module layer and the vacuum vessel. The figure also shows the results of a thin-wall calculation. It can be seen that, when the mode rotation is not significantly slowed, the magnetic flux penetrates the (inner surface of the) inner wall more effectively in the thick-wall calculation than in the thin-wall calculation.

Finally, Fig. 5 shows the torque balance diagnostic, \mathcal{T} , as a function of time. Recall that if $\mathcal{T} \approx 0$, then the plasma is in a torque-balanced state in which the electromagnetic torque at the rational surface is exactly balanced by the viscous and poloidal flow-damping torques. It can be seen that the plasma is indeed in a torque-balanced state well before and well after the occurrence of wall locking. On the other hand, the plasma is clearly not in a torque-balanced state during the time interval in which wall locking occurs, indicating that plasma inertia is playing a significant role in the wall-locking process. The figure also shows the results of a thin-wall calculation. It can be seen that the thin-wall torque balance curve is a little different than the thick-wall curve.

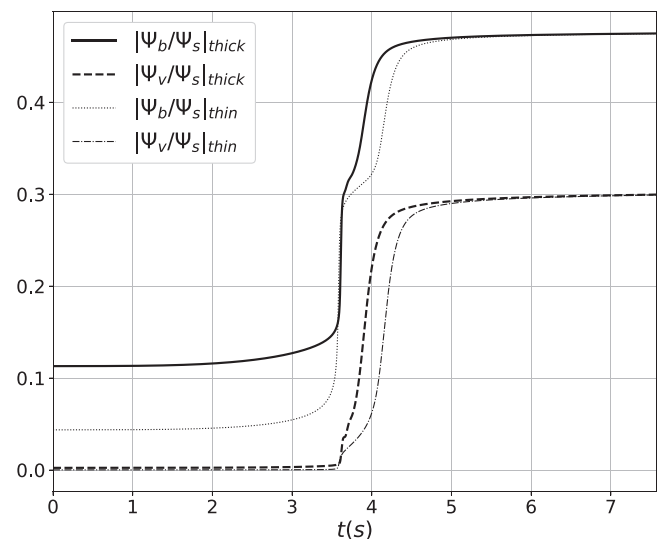


FIG. 4. Fractions of the reconnected 2/1 magnetic flux that penetrates the inner wall ($|\Psi_v/\Psi_s|$) and the outer wall ($|\Psi_b/\Psi_s|$) as functions of time. The subscripts thick and thin indicate thin-wall and thick-wall calculations, respectively.

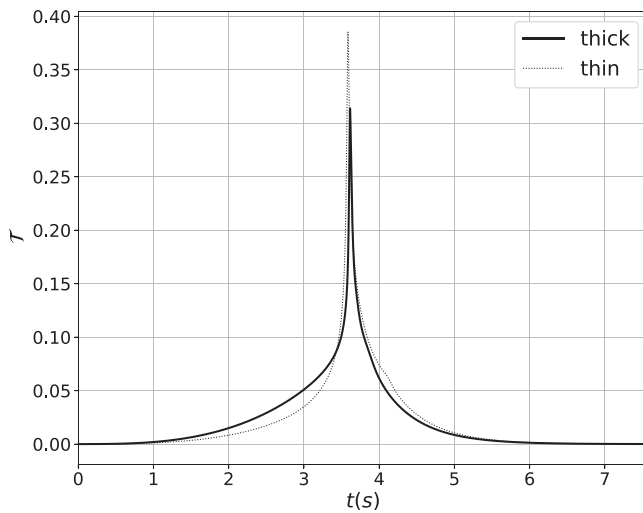


FIG. 5. Torque balance diagnostic as function of time. The subscripts thick and thin indicate thin-wall and thick-wall calculations, respectively.

C. Frequency scan

The ITER plasma parameter whose value is most difficult to predict is the plasma toroidal rotation. This uncertainty implies that the most uncertain parameter in our simulation is the natural frequency, ω_0 . Unlike most existing tokamaks, ITER will not possess an unbalanced neutral beam injection heating system that is capable of imparting significant toroidal momentum to plasma. As such, it is difficult to envisage situations in which the toroidal rotation in ITER plasmas will significantly exceed diamagnetic levels. In this situation, we expect the contribution to the natural frequency from diamagnetic levels of poloidal plasma rotation to be similar in magnitude to the contribution from toroidal plasma rotation. This observation leads to the following estimate for the natural frequency:

$$\omega_0 \sim \frac{m}{r_s} \frac{[T_e(\text{eV}) + T_i(\text{eV})]}{B_\phi L_p}, \quad (160)$$

where L_p is the pressure scale length. For the case in hand, $m = 2$, $r_s = 1.74$ m, $T_e = 5.6 \times 10^3$ eV, $T_i = 5.7 \times 10^3$ eV, $B_\phi = 5.3$ T, and $L_p = 0.9$ m.^{28,29} Thus, we obtain $\omega_0 \sim 400$ Hz. This prediction is consistent with our previous calculation, as well as the best estimates in the literature.³⁰

Figures 6 and 7 show the times required for locking of the 2/1 tearing mode to the blanket module layer and the vacuum vessel, as well as the critical island widths needed to trigger locking, calculated using our model for all likely values of the natural frequency. These calculations are identical to the calculation discussed in Secs. II A and II B, apart from the fact that ω_0 is allowed to take a range of different values. It can be seen that if the natural frequency lies below 40 Hz, then the 2/1 tearing mode is locked to the blanket module layer at birth. However, for higher values of the natural frequency, the 2/1 mode is born rotating and subsequently locks to the wall. Both the locking time and the critical island width required to trigger locking scale roughly as the square root of the natural frequency. The main results of this paper—that the locking time exceeds about 3.5 s and

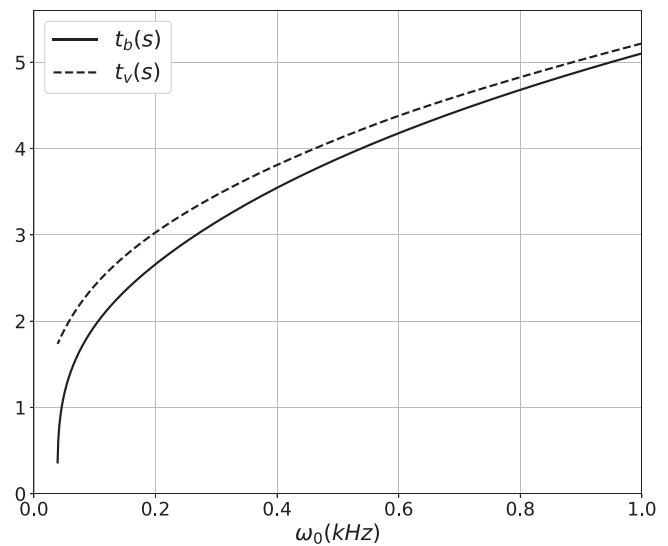


FIG. 6. Time required for 2/1 locking to the blanket module layer (t_b) and to the vacuum vessel (t_v) as functions of the natural frequency.

that the critical island width required to trigger locking exceeds about 9% of the plasma minor radius—hold unless the plasma rotation falls well below diamagnetic values.

D. Bootstrap current

Finally, we have performed some relatively crude calculations in which we attempt to include the effect of the equilibrium bootstrap current density at the 2/1 rational surface, which is estimated to be 0.074 MA/m², in the model.²⁸ We find that the bootstrap drive (due to the loss of the bootstrap current inside the magnetic separatrix of

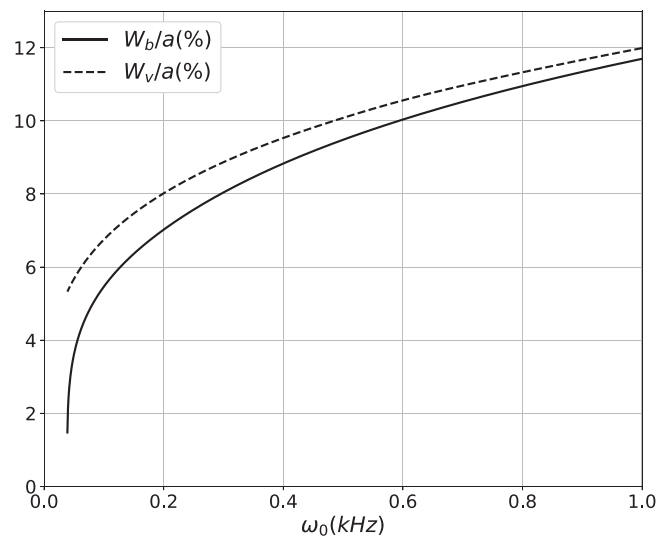


FIG. 7. Critical 2/1 island widths for locking to the blanket module layer (W_b) and to the vacuum vessel (W_v) as functions of the natural frequency.

the island chain) can reduce the locking time to as small a value as 0.5 s. On the other hand, the critical island width at which the mode locks to the wall is slightly increased to about 10% of the plasma minor radius.

IV. SUMMARY AND CONCLUSIONS

In this paper, we have simulated the locking of the 2/1 tearing mode to the wall in the ITER 15 MA inductive scenario 2 (Ref. 27) using a cylindrical asymptotic matching model.⁶ Our calculation is similar to an earlier calculation performed by La Haye *et al.*,¹⁴ but incorporates more physics. Our model takes into account the fact that ITER plasmas will effectively be surrounded by two walls; the inner blanket module layer with a time constant (which in this paper is defined as $\mu_0 r \delta / \eta$, where r , δ , and η are the wall minor radius, radial thickness, and resistivity, respectively) of about 23 ms, and the outer vacuum vessel with a time constant of about 380 ms. Our model also takes cognizance of the fact that neither the blanket module layer nor the vacuum vessel can be accurately described as thin walls (i.e., such that the wall thickness is much less than the skin-depth). Our model incorporates changes in both the plasma poloidal and the toroidal angular velocity profiles, in response to the electromagnetic braking torque that develops at the rational surface, because it turns out that neoclassical poloidal flow-damping is not strong enough to completely suppress changes in the poloidal velocity. Finally, our model accurately calculates changes in the poloidal and toroidal plasma angular velocity profiles by evolving the full angular equations of motion, taking the electromagnetic braking torque, plasma inertia, plasma viscosity, and poloidal flow-damping into account. Note that a similar, but somewhat simpler, theoretical model to that employed in this paper was successfully used to model the slowing down and locking of large amplitude $m = 1$ tearing modes to a thick wall in the MST reversed field pinch.⁷

We find that wall locking of the 2/1 tearing mode in ITER takes place in two stages. First, the mode locks to the blanket module layer and is left rotating at about 15 Hz. Next, the mode locks to the vacuum vessel and is left rotating at less than 0.5 Hz. The time required for the mode to grow from a small amplitude to sufficient one large to lock to the walls is about 3.5 s (but becomes shorter if the bootstrap current is included in the calculation). The critical island width required to trigger wall locking is about 9% of the plasma minor radius. The latter prediction is not as pessimistic as that of La Haye *et al.*, who obtained a critical island width of only 4.5% of the plasma minor radius.¹⁴ We find that about 20% of the mode frequency shift associated with wall locking is due to changes in the poloidal plasma angular velocity at the rational surface, the remaining 80% being due to changes in the toroidal angular velocity. The plasma is found to be in a torque-balanced state (i.e., one in which the electromagnetic torque at the rational surface is exactly balanced by the viscous and poloidal flow-damping torques) well before and well after the occurrence of wall locking. On the other hand, the plasma is not in a torque-balanced state during the time interval in which wall locking occurs, indicating that plasma inertia plays a significant role in the wall-locking process.

Given that the likely toroidal plasma rotation levels in ITER plasmas are very uncertain, we have repeated our calculation for a range of probable rotation levels. We find that the main results of this paper—that the locking time exceeds about 3.5 s (in the absence of the bootstrap current) and that the critical island width required to trigger

locking exceeds about 9% of the plasma minor radius—hold unless the plasma rotation falls well below diamagnetic values.

The pessimistic prediction by La Haye *et al.* that the critical island width for wall locking of the 2/1 tearing mode in ITER is only about 4.5% of the plasma minor radius¹⁴ has led Nies *et al.* to propose that that the mode be allowed to lock before an attempt is made to control it via electron cyclotron current drive localized about the rational surface (because it much easier to correctly phase the current drive to the magnetic island chain when the chain is stationary rather than when it is rotating).³¹ However, if the critical island width is actually 9% of the plasma minor radius (which is similar to the critical island width in the existing large tokamaks), then this novel idea loses some of its attractiveness.

ACKNOWLEDGMENTS

The author would like to thank R.L. La Haye for providing the ITER data. This research was directly funded by the U.S. Department of Energy, Office of Science, Office of Fusion Energy Sciences, under Contract No. DE-SC0021156.

AUTHOR DECLARATIONS

Conflict of Interest

The authors have no conflicts to disclose.

Author Contributions

Richard Fitzpatrick: Conceptualization (lead); Data curation (lead); Formal analysis (lead); Funding acquisition (lead); Writing – original draft (lead); Writing – review & editing (lead).

DATA AVAILABILITY

The data that support the findings of this study are available from the author upon reasonable request.

REFERENCES

- G. Berge, L. K. Sandal, and J. A. Wesson, *Phys. Scr.* **40**, 173 (1989).
- M. Persson and A. Bondeson, *Nucl. Fusion* **29**, 989 (1989).
- T. C. Hender, C. G. Gimblett, and D. C. Robinson, *Nucl. Fusion* **29**, 1279 (1989).
- M. F. F. Nave and J. A. Wesson, *Nucl. Fusion* **30**, 2575 (1990).
- H. Zohm, A. Kallenbach, H. Bruhns, G. Fussmann, and O. Klüber, *Europhys. Lett.* **11**, 745 (1990).
- R. Fitzpatrick, *Nucl. Fusion* **33**, 1049 (1993).
- B. E. Chapman, R. Fitzpatrick, D. Craig, P. Martin, and G. Spizzo, *Phys. Plasmas* **11**, 2156 (2004).
- P. C. de Vries, M. F. Johnson, B. Alper, P. Buratti, T. C. Hender, H. R. Koslowski, and V. Riccardo, *Nucl. Fusion* **51**, 053018 (2011).
- R. J. La Haye, A. Isayama, and M. Maraschek, *Nucl. Fusion* **49**, 045005 (2009).
- K. Ioki, V. Barabash, J. Cordier, M. Enoeda, G. Federici, B. C. Kim, I. Mazul, M. Merola, M. Morimoto, M. Nakahira *et al.*, *Fusion Eng. Des.* **83**, 787 (2008).
- G. Navratil, J. Bialek, and O. Katsuro-Hopkins, in *Second Meeting of the ITPA Topical Group on MHD, Disruption and Control, 21–23 October, 2002* (IPP, Garching, Germany, 2002).
- Y. Liu, A. Bondeson, Y. Gribov, and A. Polevoi, *Nucl. Fusion* **44**, 232 (2004).
- F. Villone, Y. Liu, G. Rubinacci, and S. Ventre, *Nucl. Fusion* **50**, 125011 (2010).
- R. J. La Haye, C. Paz-Soldan, and Y. Q. Liu, *Nucl. Fusion* **57**, 014004 (2017).
- C. G. Gimblett, *Nucl. Fusion* **26**, 617 (1986).
- H. P. Furth, J. Killeen, and M. N. Rosenbluth, *Phys. Fluids* **6**, 459 (1963).

- ¹⁷J. A. Wesson, *Nucl. Fusion* **18**, 87 (1978).
- ¹⁸R. Fitzpatrick, R. J. Hastie, T. J. Martin, and C. M. Roach, *Nucl. Fusion* **33**, 1533 (1993).
- ¹⁹P. H. Rutherford, *Phys. Fluids* **16**, 1903 (1973).
- ²⁰S. P. Hirschman and D. J. Sigmar, *Nucl. Fusion* **21**, 1079 (1981).
- ²¹Y. B. Kim, P. H. Diamond, and R. J. Groebner, *Phys. Fluids B* **3**, 2050 (1991).
- ²²R. Fitzpatrick, S.-K. Kim, and J. Lee, *Phys. Plasmas* **28**, 082511 (2021).
- ²³R. Fitzpatrick, *Plasma Physics: An Introduction* (CRC Press, Boca Raton, FL, 2015).
- ²⁴R. J. Hastie, F. Militello, and F. Porcelli, *Phys. Rev. Lett.* **95**, 065001 (2005).
- ²⁵R. Fitzpatrick, E. Rossi, and E. P. Yu, *Phys. Plasmas* **8**, 4489 (2001).
- ²⁶R. Fitzpatrick, *Phys. Plasmas* **29**, 032507 (2022).
- ²⁷H. van den Brand, M. R. de Baar, N. J. Lopes Cardozo, and E. Westerhof, *Plasma Phys. Controlled Fusion* **54**, 094003 (2012).
- ²⁸L. Urso, *Modelling and Experiments on NTM Stabilisation at ASDEX Upgrade* (Ludwig-Maximilians-Universität München, Munich, Germany, 2009).
- ²⁹A. R. Polevoi, S. Y. Medvedev, V. S. Mukhatov, A. S. Kukushkin, Y. Murakami, M. Shimada, and A. A. Ivanov, *J. Plasma Fusion Res. Ser.* **5**, 82 (2002); available at http://www.jspf.or.jp/PPFRS/PDF/Vol5/jpfrs2002_05-082.pdf.
- ³⁰C. Chrystal, B. A. Grierson, S. R. Haskey, A. C. Sontag, F. M. Poli, M. W. Shafer, and J. S. deGrassie, *Nucl. Fusion* **60**, 036003 (2020).
- ³¹R. Nies, A. H. Reiman, and N. J. Fisch, *Nucl. Fusion* **62**, 086044 (2022).